J Mater Sci (2009) 44:3428–3437
DOI 10.1007/s10853-009-3456-1

Experimental investigation of mixed-mode fracture behaviour of woven laminated composite

Masood Nikbakht · Naghdali Choupani

Received: 20 December 2008 / Accepted: 31 March 2009 / Published online: 17 April 2009

Abstract In this paper, the mixed-mode interlaminar fracture behaviour of woven carbon-epoxy composite was investigated based on experimental and numerical analyses. A modified version of Arcan specimen was employed to conduct a mixed mode fracture test using a special loading device. A full range of mixed-mode loading conditions including pure mode-I and pure mode-II loading were created and tested. This test method has a simple procedure, clamping/unclamping the specimens are easy to achieve and only one type of specimen is required to generate all loading conditions. Also, finite element analysis was carried out for different loading conditions in order to determine correction factors needed for fracture toughness calculations. Interlaminar fracture toughness was determined experimentally with the modified version of the Arcan specimen under different mixed-mode loading conditions. Results indicated that the interlaminar cracked specimen is tougher in shear loading condition and weaker in tensile loading condition. Response of woven carbon-epoxy composite was also investigated through several criteria and the best criterion was selected. The interlaminar fracture surfaces of the carbon-epoxy composite under different mixed-mode loading conditions are examined by scanning electron microscopy (SEM).

M. Nikbakht · N. Choupani (✉)
Mechanical Engineering Department, Sahand University of Technology, P.O. Box: 51335-1996, Tabriz, Iran
e-mail: Choupani@sut.ac.ir; nchupaani@yahoo.com

M. Nikbakht
e-mail: m_nikbakht@sut.ac.ir

Introduction

Characterizing interlaminar fracture toughness is an effective factor in determining the fracture of composite materials as failures in composite materials occur mainly due to interlaminar fracture, also called delamination, between laminates. In recent years, many test methods have been proposed by many researchers to determine interlaminar fracture toughness for three modes of loading (I, II and III) and also under mixed-mode conditions. Some of these include: the double cantilever beam (DCB) test, the end-notched flexure (ENF) specimen, the mixed-mode flexure (MMF) test, the end loaded split (ELS) specimen, the single leg bending (SLB) specimen, the crack lap shear (CLS) test, the edge delamination tension (EDT) specimen, the asymmetric double cantilever beam and the Richard specimen [1–23]. The double cantilever beam (DCB) test is the most widely used method for measuring mode-I (opening) fracture toughness (Fig. 1a). The end-notched flexure (ENF) has emerged as one of the most convenient mode-II (shear) type cracking test (Fig. 1b). However, deep understanding of the fracture behaviour of adhesively bonded joints, and particularly under mixed-mode loading conditions, is needed in order to fully achieve the benefits of adhesive bonding.

Various attempts have been made to characterize fracture toughness under mixed-mode loading conditions, but mostly beam type specimens were used. If the so-called end loaded split (ELS) specimen is loaded by the upper arm, mixed-mode loading conditions at the crack tip are achieved (Fig. 1c). The mixed-mode bending (MMB) test specimens has been proposed by combining the schemes used for DCB and ENF tests to study mixed-mode fracture toughness (Fig. 1d). However, for these test methods there are problems to create a wide range of mixed-mode ratios which limit their usefulness. Also, different beam type

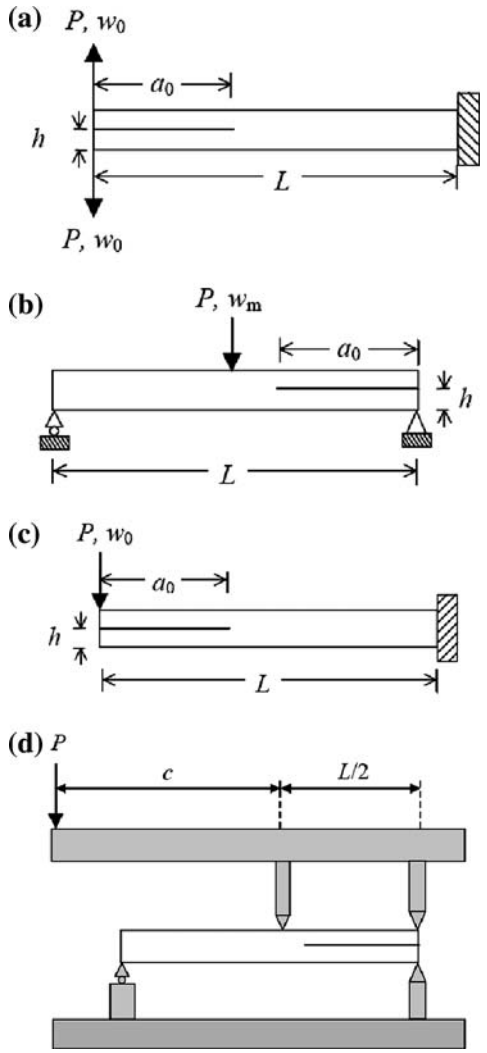

Fig. 1 Most applicable configurations for delamination testing **a** double cantilever beam (DCB) for mode-I, **b** end-notched flexure beam (ENF) for mode-II, **c** end load split (ELS) for mixed mode and **d** mixed mode bending (MMB) for mixed mode loading

specimens would be required in order to obtain reliable results for fracture toughness in pure mode-I, pure mode-II and mixed-mode loading conditions. It is therefore necessary to develop other test methods to evaluate the mixed-mode fracture toughness under all in-plane loading conditions starting from pure mode-I to pure mode-II. Another type of specimen for studying mixed-mode fracture toughness is the Arcan specimen (Fig. 2).

Only limited work could be found in the literature regarding the mixed-mode interlaminar fracture behaviour of composite materials using Arcan specimen [6–10]. The geometry of the modified Arcan test fixture and specimen under investigation is shown in Fig. 2. Originally used for testing of composite specimens by [6, 7], the fixture was modified for mixed-mode cohesive, interfacial and interlaminar fracture tests. In particular, a number of holes and

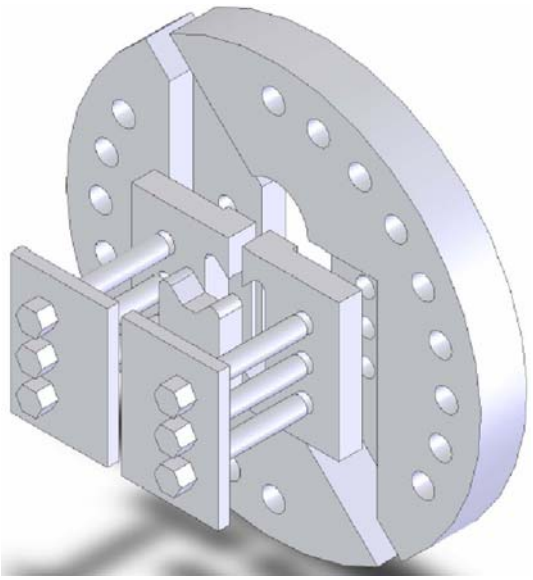

Fig. 2 Fixture and Arcan specimen and mounting procedure

rod inserts were added to stiffen the specimen–fixture connection. The pinhole locations on the outer edge of the fixture provide a range of loading angles. The specimen is attached to the fixture by three pins at each end. The specimen is loaded by pulling apart grips of the fixture at a pair of grip holes on the opposite sides of a radial line. By varying the loading angle α ($\alpha = 0°$, 15°, 30°, 45°, 60°, 75°, 90°), all mixed-mode conditions starting from pure mode-I to pure mode-II can be created and tested. Jurf and Pipes [8] investigated interlaminar fracture characteristics of graphite/epoxy composite material under mode-I, mode-II and mixed-mode loadings (for only two mixed-mode loading angles) to examine a mixed-mode interlaminar fracture criterion. They found that G_{IIC} was nine times more than G_{IC}. It was not clear whether they used finite correction for composite materials, as using homogeneous material geometrical factors may lead to incorrect results. Yoon and Hong [9] studied the interlaminar fracture behaviour of graphite/epoxy composite material under mode-I, mode-II and mixed-mode deformations using DCB, ENF and Arcan specimens. They found that mode-II interlaminar fracture toughness for the ENF specimen was about the same for the Arcan test specimen and in contrast, mode-I interlaminar fracture toughness for the DCB specimen was larger than that for the Arcan specimen.

In this research, mixed-mode fracture experiments were conducted to determine the fracture toughness of a woven carbon-epoxy composite material. The stress intensity calibration was obtained by finite element analysis using the finite correction factors method. The mixed-mode fracture criteria were determined and fracture surfaces obtained at different loading angles were discussed.

Theoretical backgrounds

The main problem of predicting the failure of composite materials is to characterize the resistance to delamination in terms of interlaminar fracture toughness especially under mixed-mode loading conditions. Linear elastic fracture mechanics has been found as a useful tool for investigating of interlaminar cracks in composite materials. It is assumed that the specimens are made of orthotropic linear elastic material defined by the generalized Hook's law. For many composites, crack growth is self-similar because of delamination and this leads to partition G value into mode-I and mode-II. The energy release rates for an orthotropic material with the crack line parallel to the principal orthotropic direction which coincides with the fibre orientation can be calculated from the following relationships [6–10]:

$$G_{\mathrm{I}} = \frac{K_{\mathrm{I}}^2}{E_{\mathrm{I}}} \quad G_{\mathrm{II}} = \frac{K_{\mathrm{II}}^2}{E_{\mathrm{II}}} \tag{1}$$

where E_{I} and E_{II} are effective module, and K_{I} and K_{II} are mode-I and mode-II stress intensity factors, respectively. It is assumed that the specimens are orthotropic linear elastic material and effective module E_{I} and E_{II} are defined as the following [10].for plane strain conditions:

$$E_{\mathrm{I}} = \sqrt{\frac{2}{a_{11}a_{22}}}\frac{1}{\sqrt{\sqrt{\frac{a_{22}}{a_{11}}}+\frac{2a_{12}+a_{66}}{2a_{11}}}} \tag{2}$$

$$E_{\mathrm{II}} = \frac{\sqrt{2}}{a_{11}}\frac{1}{\sqrt{\sqrt{\frac{a_{22}}{a_{11}}}+\frac{2a_{12}+a_{66}}{2a_{11}}}} \tag{3}$$

and for plane stress conditions:

$$E_{\mathrm{I}} = \sqrt{\frac{2}{b_{11}b_{22}}}\frac{1}{\sqrt{\sqrt{\frac{b_{22}}{b_{11}}}+\frac{2ab_{12}+b_{66}}{2b_{11}}}} \tag{4}$$

$$E_{\mathrm{II}} = \frac{\sqrt{2}}{b_{11}}\frac{1}{\sqrt{\sqrt{\frac{b_{22}}{b_{11}}}+\frac{2b_{12}+b_{66}}{2b_{11}}}} \tag{5}$$

where the terms of the nonzero entries a_{ij} of the orthotropic compliance matrix are defined in terms of the engineering elastic constants and the terms of the constants b_{ij} are defined in terms of the following nonzero entries a_{ij} of the orthotropic compliance matrix:

$$b_{ij} = a_{ij} - \frac{a_{i3}a_{j3}}{a_{33}} \cdots (i,j = 1,2,4,5,6) \tag{6}$$

The purpose of fracture toughness testing is to determine the value of the critical stress intensity factor. This material property is used to characterize the resistance to fracture in the design of structural members. Due to presence of weak planes between the layers of a composite laminate, interlaminar fractures are often subjected to a mixed-mode stress field. The stress intensity factors ahead of the interlaminar crack tip for a modified version of Arcan specimen can be calculated by using the following equations [8–10]:

$$K_{\mathrm{I}} = \frac{P_C\sqrt{\pi a}}{wt} f_1\left(\frac{a}{w}\right) \tag{7}$$

$$K_{\mathrm{II}} = \frac{P_{\mathrm{C}}\sqrt{\pi a}}{wt} f_2\left(\frac{a}{w}\right) \tag{8}$$

where P_{C} is the critical load at fracture, w is specimen length, t is the specimen thickness and a is crack length. In turn K_{I} and K_{II} are obtained using geometrical factors $f_1(a/w)$ and $f_2(a/w)$, respectively [24].

Finite element analysis

The stress intensity factors K_{I}, K_{II} and K_{III} play an important role in linear elastic fracture mechanics. The stress intensity can be related to the energy release rate (the J-integral) for a linear elastic material through:

$$J = \frac{1}{8\pi} K^T \cdot B^{-1} \cdot K \tag{9}$$

where $K = [K_{\mathrm{I}} \quad K_{\mathrm{II}} \quad K_{\mathrm{III}}]^T$ and B is called the pre-logarithmic energy factor matrix. In order to calculate stress intensity factors, interaction integral method is commonly used. In general, the J-integral for a given problem can be written as

$$J = \frac{1}{8\pi}\left[K_{\mathrm{I}}B_{11}^{-1}K_{\mathrm{I}} + K_{\mathrm{I}}B_{12}^{-1}K_{\mathrm{II}} + K_{\mathrm{I}}B_{13}^{-1}K_{\mathrm{III}} + (\text{Terms not involving } K_{\mathrm{I}})\right] \tag{10}$$

where I, II, III correspond to 1, 2, 3 indicating the components of B. The J-integral for an auxiliary, pure mode I, crack-tip field with stress intensity factor k_{I}, is defined as

$$J_{\mathrm{aux}}^{\mathrm{I}} = \frac{1}{8\pi} k_{\mathrm{I}} \cdot B_{11}^{-1} \cdot k_{\mathrm{I}} \tag{11}$$

Superposing the auxiliary field on to the actual field yields

$$J_{\mathrm{tot}}^{\mathrm{I}} = \frac{1}{8\pi}\left[(K_{\mathrm{I}}+k_{\mathrm{I}})B_{11}^{-1}(K_{\mathrm{I}}+k_{\mathrm{I}}) + 2(K_{\mathrm{I}}+k_{\mathrm{I}})B_{12}^{-1}K_{\mathrm{I}} + 2(K_{\mathrm{I}}+k_{\mathrm{I}})B_{13}^{-1}K_{\mathrm{III}} + (\text{Terms not involving } K_{\mathrm{I}} \text{ or } k_{\mathrm{I}})\right] \tag{12}$$

Since the terms not involving K_{I} or k_{I} in J_t^1 are equal, the interaction integral can be defined as

$$J_{\text{int}}^{\text{I}} = J_{\text{tot}}^{I} - J - J_{\text{aux}}^{\text{I}} = \frac{k_{\text{I}}}{4\pi}\left(B_{11}^{-1}K_{\text{I}} + B_{12}^{-1}K_{\text{II}}BK + B_{13}^{-1}K_{\text{III}}\right) \tag{13}$$

If the calculations are repeated for mode II and mode III, a linear system of equation results:

$$J_{\text{int}}^{a} = \frac{k_{\alpha}}{4\pi}B_{\alpha\beta}^{-1}K_{\beta} \tag{14}$$

If the k_{α} are assigned unit values, the solution of the above equation leads to

$$K = 4\pi B \cdot J_{\text{int}} \tag{15}$$

where $J_{\text{int}} = \left[J_{\text{int}}^{\text{I}}\ J_{\text{int}}^{\text{II}}\ J_{\text{int}}^{\text{III}}\right]^{T}$. Based on the definition of the J-integral, the interaction integrals J_{int}^{α} can be expressed as

$$J_{\text{int}}^{\alpha} = \text{Lim}_{\Gamma\to 0}\int_{\Gamma} n \cdot M^{\alpha} \cdot q\text{d}\Gamma \tag{16}$$

with M^{α} given as

$$M^{\alpha} = \sigma : \varepsilon_{\text{aux}}^{\alpha}\text{I} - \sigma \cdot \left(\frac{\partial u}{\partial x}\right)_{\text{aux}}^{\alpha} - \sigma_{\text{aux}}^{\alpha} \cdot \frac{\partial u}{\partial x} \tag{17}$$

The subscript aux represent three auxiliary pure mode I, mode II and mode III crack-tip fields for α = I, II, III, respectively. Γ is a contour that lies in the normal plane at position s along the crack front, beginning on the bottom crack surface and ending on the top surface (Fig. 3). The limit $\Gamma \to 0$ indicates that Γ shrinks onto the crack tip. To evaluate these integrals, ABAQUS defines the domain in terms of rings of elements surrounding the crack tip [25].

The numerical analyses were performed with ABAQUS finite element software under a constant load of 1000 N. As mesh pattern of the entire apparatus can be observed in Fig. 4a, the entire apparatus was modelled using eight node collapsed quadrilateral elements and the mesh was refined around crack tip (Fig. 4b), so that the smallest element size found in the crack tip elements was approximately 0.25 mm. Linear elastic finite element analysis was performed under a plain strain condition using $1/\sqrt{r}$ stress field singularity. To obtain a $1/\sqrt{r}$ singularity term of the crack tip stress field, the elements around the crack tip were focused on the crack tip and the mid-side nodes were moved to a quarter point of each element side.

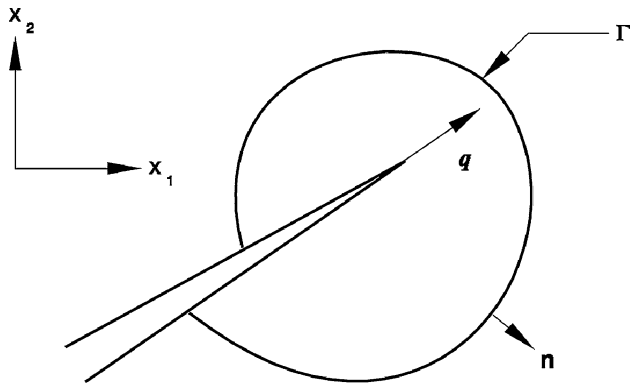

Fig. 3 Contour for calculating J-integral

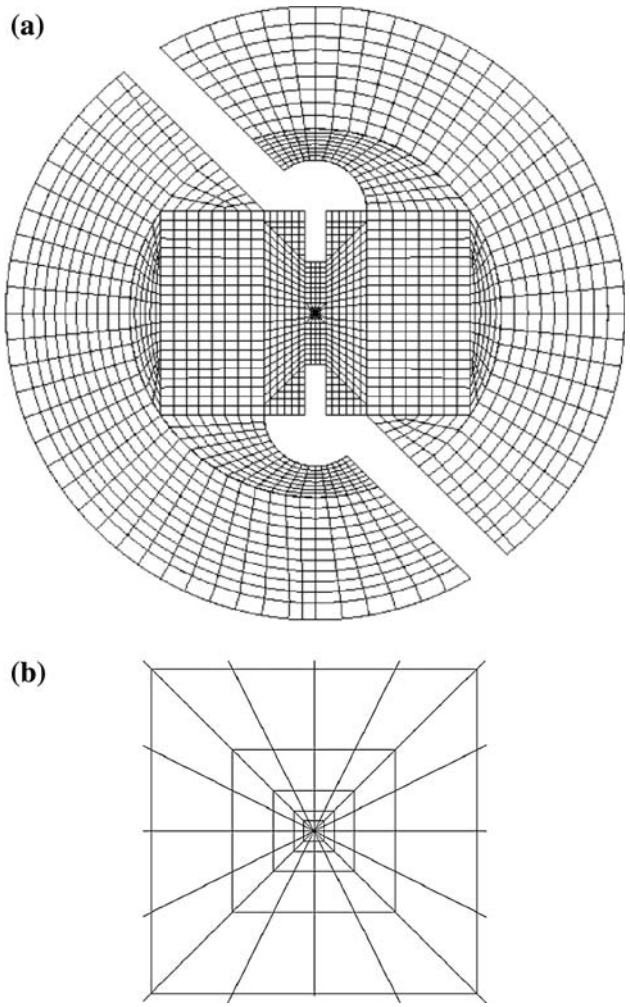

Fig. 4 **a** Finite element mesh pattern, **b** refined mesh around the crack tip

Test method and setup

Experiments were conducted using a modified Arcan specimen, in which a wide range of mode ratios was obtained by varying the loading angle. The aim of the experiments was to determine the interlaminar fracture toughness of woven carbon-epoxy composite material. In the experiment, a plate consisting of 130 plies of woven carbon-epoxy prepergs, in order to obtain a plate thickness of approximately 26 mm were used. During the lay up of prepergs by hand to the required number of plies, a non-adhering film was placed between the central plies in order to introduce a starter crack. The composite plates were

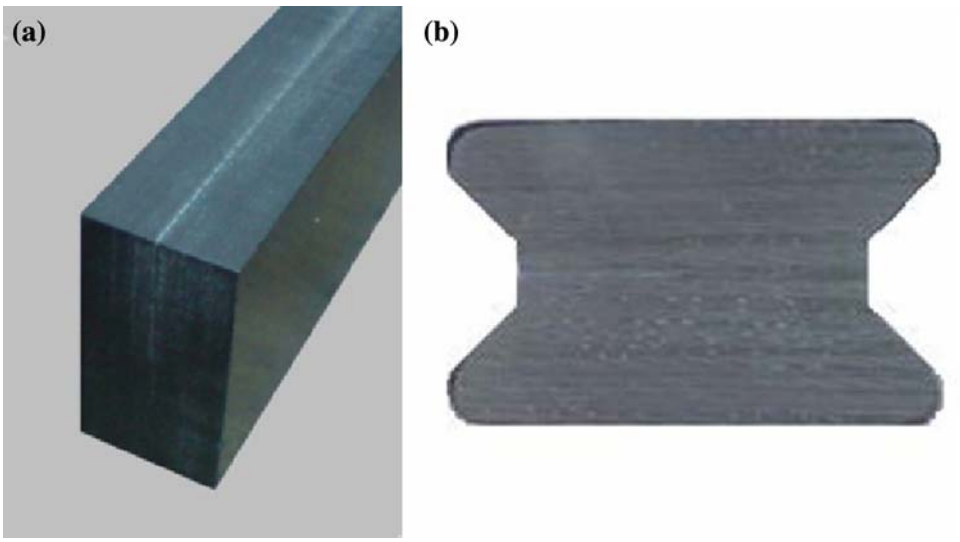

Fig. 5 **a** Primitive specimen, **b** specific machined specimen

Table 1 Elastic properties of woven carbon-epoxy composite

E_1 (GPa)	37.05
E_2 (GPa)	37.05
E_3 (GPa)	7.6
G_{12} (GPa)	5
G_{13} (GPa)	2.76
G_{23} (GPa)	2.76
v_{12}	0.04
v_{13}	0.36
v_{23}	0.36

produced using a hot press. Curing of woven carbon-epoxy composite was performed at elevated temperature and pressure under manufacturer's specifications. The specimens were cut with a diamond wheel and machined to the dimensions of approximately 30 × 10 × 26 mm (Fig. 5b). Elastic constants of woven carbon-epoxy used in this investigation are summarized in Table 1. For woven carbon-epoxy composite material, 1 is the direction parallel to the crack and 2 and 3 are the directions normal to the crack, while the direction of the crack coincides with the fibre direction. The composite strip was attached into two-part clamps. The modified Arcan test specimen and loading fixture (composed of a pair of grips) are shown in Fig. 6. The specimen was attached to the fixture by three pins at each end. The specimen is loaded by pulling apart grips of the fixture at a pair of grip holes on the opposite sides of a radial line. By varying the loading angle α ($\alpha = 0°$, 15°, 30°, 45°, 60°, 75°, 90°), all mixed-mode conditions starting from pure mode-I to pure mode-II can be created and tested. Fracture tests were conducted by controlling the constant displacement rate of 0.5 mm/min and the fracture loads and displacements were recorded. All tests were carried out using an Instron testing machine. Tests were repeated 3 times for every loading angle.

Results and discussions

In order to assess stress intensity factors at fracture K_I and K_{II} using Eqs. 7 and 8, geometrical factors or non-dimensional stress intensity factors $f_I(a/w)$ and $f_{II}(a/w)$ for both pure mode-I and pure mode-II loadings were determined. The a/w ratio was varied between 0.1 and 0.8 at 0.1 intervals and a fifth order polynomial was fitted through finite element analysis. From the finite element results, closed-form solutions using least square fitting for a modified Arcan specimen can be derived as (Fig. 7):

$$\begin{aligned} f_I\left(a/w\right) &= 533.1\left(a/w\right)^5 - 965.4\left(a/w\right)^4 + 681.1\left(a/w\right)^3 \\ &\quad - 218.0\left(a/w\right)^2 + 33.98\left(a/w\right) - 1.146 \\ f_{II}\left(a/w\right) &= 21.96\left(a/w\right)^5 - 44.89\left(a/w\right)^4 + 39.22\left(a/w\right)^3 \\ &\quad - 17.39\left(a/w\right)^2 + 5.963\left(a/w\right) - 0.18 \end{aligned} \tag{18}$$

Here a/w is the crack length ratio, where a is the rack length and w is the specimen length. Figure 7 shows the changes in non-dimensional stress intensity factors $f_I(a/w)$ (for loading angle LA = 0°) and $f_{II}(a/w)$ (for loading angle LA = 90°) due to change in the crack length. Although the mode-I non-dimensional stress intensity factor value changes largely due to the change in the crack length ratio, the mode-II value does not change markedly. Therefore, the increase of the crack length leads to a reduction of fracture resistance.

It is also of interest to compare the non-dimensional stress intensity factors for different loading angles. From Fig. 8, it can be seen that as mode-II loading contribution increases, the mode-I stress intensity factor decreases and the mode-II stress intensity factor increases. Adherends with different properties were found to have significant effects on the stress intensity factors that decrease as the adherend modulus increases. It is also seen that for loading

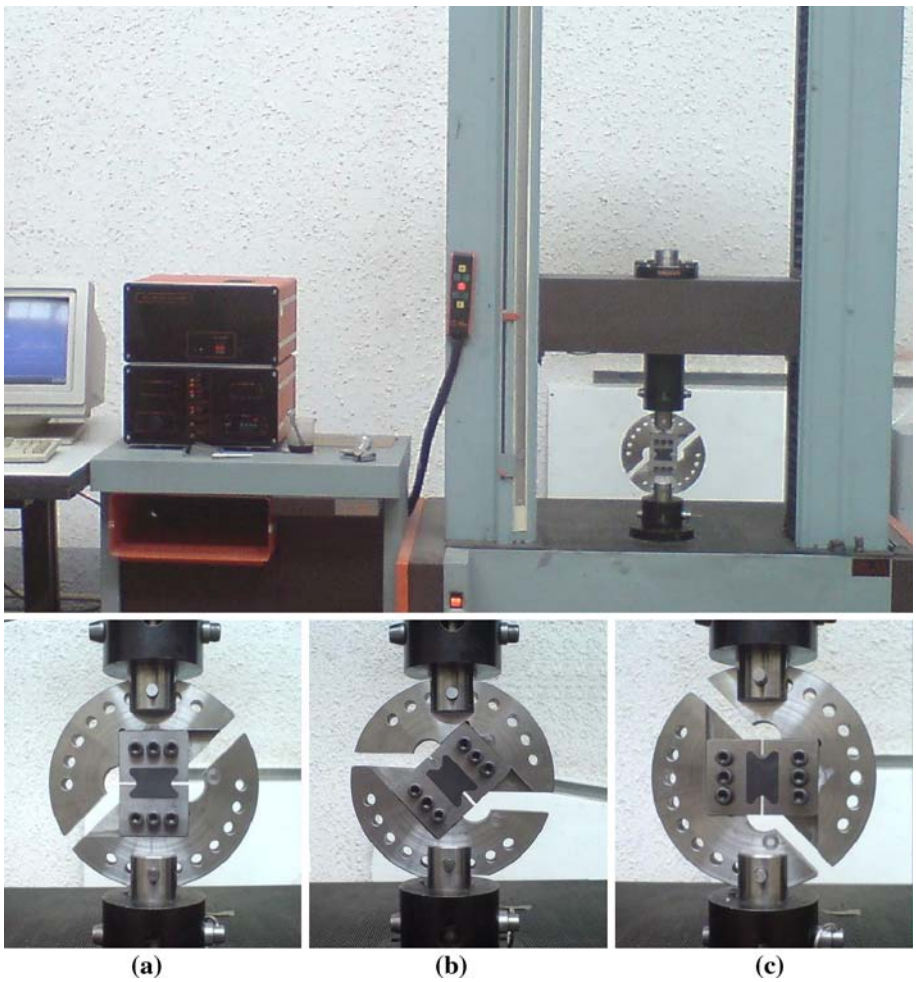

Fig. 6 An overview of loading device and setup: **a** pure mode-I, **b** mixed mode, **c** pure mode-II

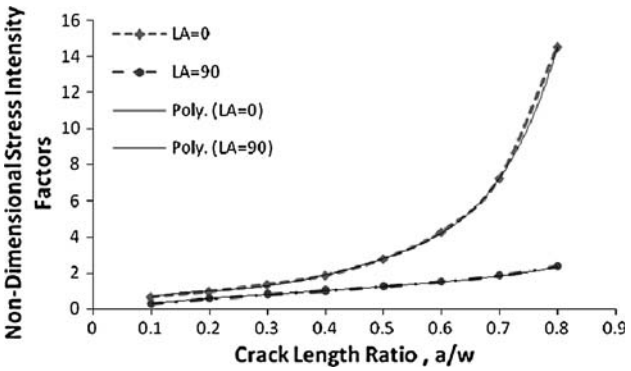

Fig. 7 Non-dimensional stress intensity factors versus crack length of woven carbon-epoxy composite material

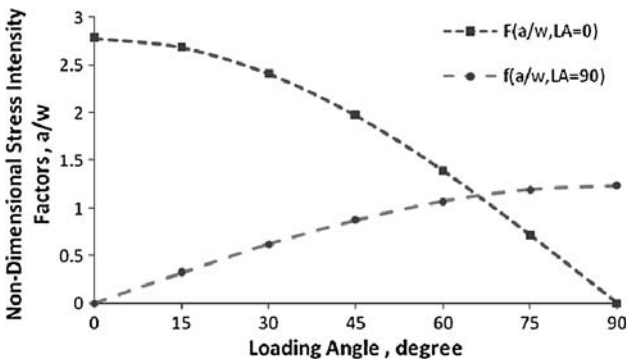

Fig. 8 Non-dimensional stress intensity factor versus loading angle of woven carbon-epoxy composite for the crack length 15 mm

angles $\alpha \leq 60°$, the mode-I fracture becomes dominant. For $\alpha \geq 75°$ mode-II fracture becomes dominant.

In Fig. 9, strain energy release rates G_I and G_{II} obtained by Eq. 1 and the total strain energy release rate obtained by $G_T = G_I + G_{II}$ are compared for a constant value of the load $P = 1000$ N. It is seen that for loading angles $\alpha \leq 60°$ the mode-I strain energy release rate is maximum and as loading angle increases, G_I decreases and G_{II} increases. For $\alpha \geq 75°$ mode-II fracture becomes dominant. The total strain energy release rate under mixed-mode loading conditions decreases with the loading angle. Therefore, the increase of the mode-II loading contribution leads to a reduction in the total strain energy release rate.

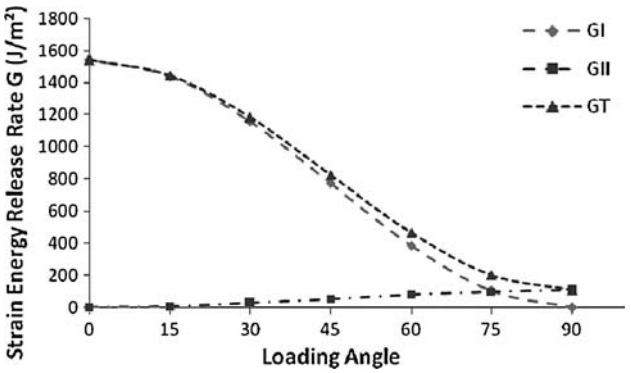

Fig. 9 Strain energy release rate of mode-I (G_I), mode-II (G_{II}) and total strain energy (G_T) versus loading angle

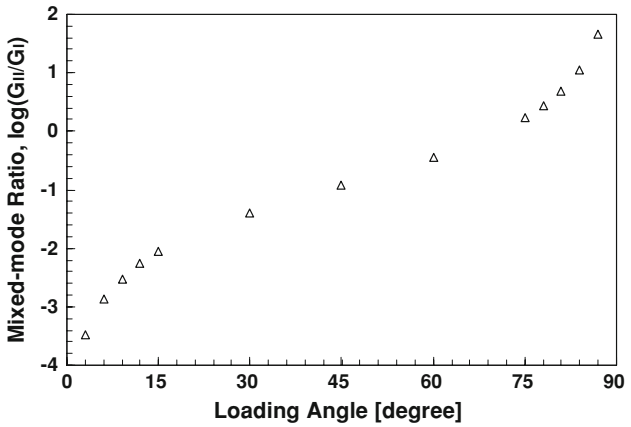

Fig. 10 The ratio of mode-II to mode-I, G_{II}/G_I, in logarithmic scale versus loading angle

The relationship between the mixed-mode ratios of strain energy release rates and the loading angles α is shown in Fig. 10. For loading angles close to pure mode-I loading, very high ratios of mode-I to mode-II are dominant. The ratios of strain energy release rates close to pure mode-II loading exhibit the opposite trend. As expected, it is confirmed that by varying the loading angle of the Arcan specimen, pure mode-I, pure mode-II and a wide range of mixed-mode loading conditions can be created and tested.

Fracture tests were performed with a universal tensile machine under a loading speed of 0.5 mm per minute. Tests were repeated at least three times for each loading angle. Load-displacement curves were used to generate average fracture load for each loading angle as shown in Table 2. The interlaminar fracture toughness was determined experimentally with the modified version of the Arcan specimen under different mixed-mode loading conditions. Average values of mixed-mode interlaminar critical stress intensity factors for woven carbon-epoxy composite are summarized in Table 3. $(K_I)_C$ increases until $\alpha = 60^\circ$ and then decreases and $(K_{II})_C$ increases as the mode-II loading contribution, i.e. as α increases from 0 to

Table 2 Average critical mixed-mode interlaminar fracture loads P_C (N) for woven carbon-epoxy composite with crack length 15 mm

	Loading angles						
	0	15	30	45	60	75	90
Critical loads							
1	500	540	560	730	1080	1800	2200
2	480	480	600	710	1210	1820	1980
3	490	520	590	725	1150	1730	2150
Average	490	513.3	583.3	721.7	1146.7	1783.3	2110

Table 3 Average interlaminar critical stress intensity factors (K_C) (MPa $m^{1/2}$) for woven carbon-epoxy composite with crack length 15 mm

	Loading angles						
	0	15	30	45	60	75	90
Stress intensity factors							
K_{IC}	0.985	0.997	1.017	1.027	1.154	0.925	
K_{IIC}		0.118	0.261	0.456	0.888	1.541	1.888

90°. It is seen that for loading angles $\alpha \leq 60^\circ$, the mode-I contribution is greater than that of mode-II and the opening-mode fracture becomes dominant. For loading angles $\alpha \geq 75^\circ$, there is an opposite trend and the shearing mode fracture becomes dominant. From Table 3, it can be seen that the shearing-mode ($\alpha = 90^\circ$) interlaminar stress intensity factor is larger than the opening-mode ($\alpha = 0^\circ$) interlaminar stress intensity factor. This means that the interlaminar cracked specimen is tougher in shear loading conditions and weaker in tensile loading conditions. Interlaminar fracture toughness measurements for the modified Arcan specimen under pure mode-I loading showed the average fracture toughness of $K_{IC} = 0.985\ (\mathrm{MPa\,m^{1/2}})$ for woven carbon-epoxy composite material. For pure mode-II loading using modified Arcan specimen, the average fracture toughness for woven carbon-epoxy composite material was found to be $K_{IIC} = 1.888\ (\mathrm{MPa\,m^{1/2}})$. Strain energy release rate values are shown in Table 4. The opening and shearing mode critical interlaminar strain energy release rates were found approximately $G_{IC} = 109.15\,\mathrm{J/m^2}$ and $G_{IIC} = 154.87\,\mathrm{J/m^2}$ which confirms that woven carbon-epoxy composite material is tougher is shearing mode.

It is well known that the interlaminar fracture energy under mode-II loading is different from that under mode-I loading. For the situation under mixed-mode loading, there is an interaction between the two fracture modes and it is necessary to find a relationship between mode-I and mode-II stress intensity factors. It is generally proposed in the form of,

Table 4 Average interlaminar critical strain energy release rate (G_C) (J/m^2) for woven carbon-epoxy composite with crack length 15 mm

	Loading angles						
	0	15	30	45	60	75	90
Fracture toughness							
G_{IC}	109.15	112.07	116.38	118.72	149.99	96.32	
G_{IIC}		0.61	2.95	9.04	34.28	103.02	154.87
G_T	109.15	112.68	119.34	127.72	184.29	199.35	154.87

$$\left(\frac{(G_I)_C}{G_{IC}}\right)^m + \left(\frac{(G_{II})_C}{G_{IIC}}\right)^n = 1 \tag{19}$$

Several studies have been conducted to obtain a suitable description of mixed-mode fracture behaviour in composites [2, 8–11, 22]. It is generally proposed in the form of Eq. 19. Jurf and Pipes [8] reported that the quadratic form of $m = 2$ and $n = 2$ is suitable for mixed-mode fracture criteria of ASI/3501-6 graphite/epoxy composite material. Yoon and Hong [9] found that a relation of the form $m = 2$ and $n = 3$ provided a better fitting of the experimental data. The interlaminar fracture toughness was determined experimentally with the modified version of the Arcan specimen for woven carbon-epoxy composite under different mixed-mode loading conditions. The average values of mixed-mode fracture toughness data are summarized in Table 4. A failure criterion was developed by plotting the average fracture toughness data on a non-dimensional diagram (Fig. 11). In this study, the fracture criterion was written in terms of the pure-mode fracture toughness, modulus values and an arbitrary constant γ. The γ constant can be chosen to model a great variety of material responses. The failure envelope can be concaved G^m_{IC} versus G^m_{IIC}. The arbitrary constant of γ, calculated through curve fitting and least square method was determined as $\gamma = 25.05$.

$$G^m_{IC} + G^m_{IIC} = (G_{IC} - G_{IIC})e^{\gamma(1-N)} + G_{IIC}$$
$$N = \sqrt{1 + \frac{G^m_{IIC}}{G^m_{IC}}\sqrt{\frac{E_{11}}{E_{22}}}} \tag{20}$$

The mode-I interlaminar fracture surfaces were examined using a scanning electron microscope (SEM). Scanning electron microscopy (SEM) of fracture surfaces of the mode-I specimens are shown in Fig. 12a and b. Figure 12a shows the fractograph of the mode-I fracture of the initiation area taken just beyond the precrack insert film of the woven carbon-epoxy composite. Therefore, the fracture surfaces show the first increment of interlaminar crack growth which corresponds to the measured fracture toughness. The mode-I fracture surface is indicative of a brittle cleavage failure with relatively smooth and flat matrix fracture (12-A) and shows debonding between fibre and matrix (12-B), which would explain the low mode-I fracture toughness. Figure 12b shows the fractograph of a

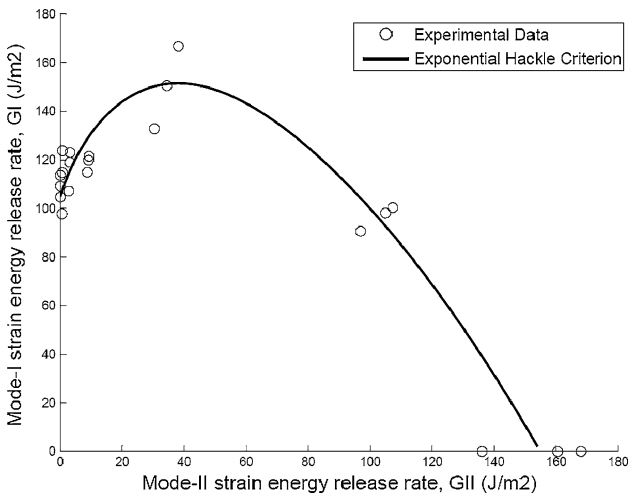

Fig. 11 Mixed-mode interlaminar fracture criterion of woven carbon-epoxy composite with the crack length 15 mm

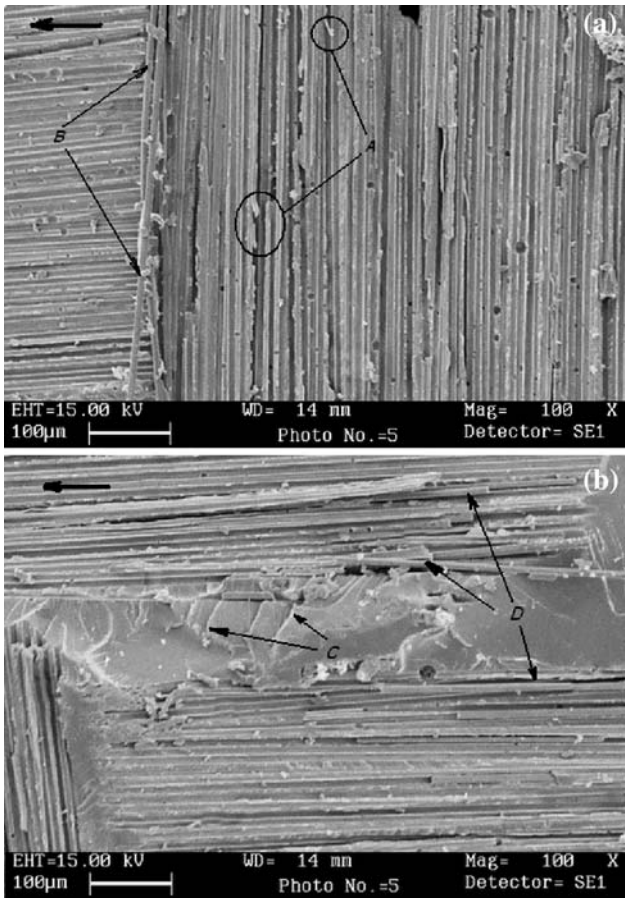

Fig. 12 **a** Initiation fracture surface, **b** propagation fracture surface of pure opening mode

mode-I fracture of the propagation area. Its characteristic is overall flatness (12-D) on the matrix fracture (12-C).

SEM micrographs show that the fracture surfaces of the woven carbon-epoxy composite change with mixed-mode ratio. Figure 13a and b shows the interlaminar fracture surfaces at mixed-mode loading conditions ($\alpha = 45°$) for the woven carbon-epoxy composite. As discussed earlier, at pure mode-I the fracture surface was very flat indicating a brittle cleavage fracture which would explain the low mode-I fracture toughness. As mode-II loading contribution is added, the fracture surfaces become rougher as seen in the micrograph taken just after the precrack insert film (13-B) under mixed-mode ($\alpha = 45°$) loading conditions. Troughs (13-E) and hackles (13-D) have appeared where fibres have been pulled away from the matrix indicating interfacial failure. Hackles are regions of the matrix deformation between adjacent fibres that are lifted up parallel to one another and tend to slant in the same direction over the entire surface. Fracture surfaces showed evidence of some distributed pores and voids (13-A). Some fibres were peel out which show the presence of mode-I component (13-F). The characteristic of the fracture surface is the traces of fibres in the resin regions (13-C) combined with voids and debonded fibres.

The observations of the mode-II fracture surfaces were carried out with scanning electron microscopy (SEM). SEM of fracture surfaces of the mode-II specimens are shown in Fig. 14a and b. A scanning electron micrograph of the area at the rear of the crack tip of the fracture surface of the mode-II specimen is shown in Fig. 14a. Everywhere on the fracture surface of the specimens, broken fibres (14-A) were observed, as the marks of fibre-matrix debonding and hackles accompanied by fragmentation of the matrix phase (14-B). Hackles are regions of the matrix deformation between adjacent fibres that are lifted up parallel to one another and tend to slant in the same direction over the entire surface. Figure 14b shows the fractograph of a mode-II fracture at the propagation area. Its characteristic is numerous inclined hackles of the matrix fracture and troughs (14-C) where fibres have been pulled away (14-D) from the matrix indicating interfacial failure. However, due to the large relative motion in mode-II loading, the fracture surface was rough and more voids, debonded particles and traces of bridging fibres were

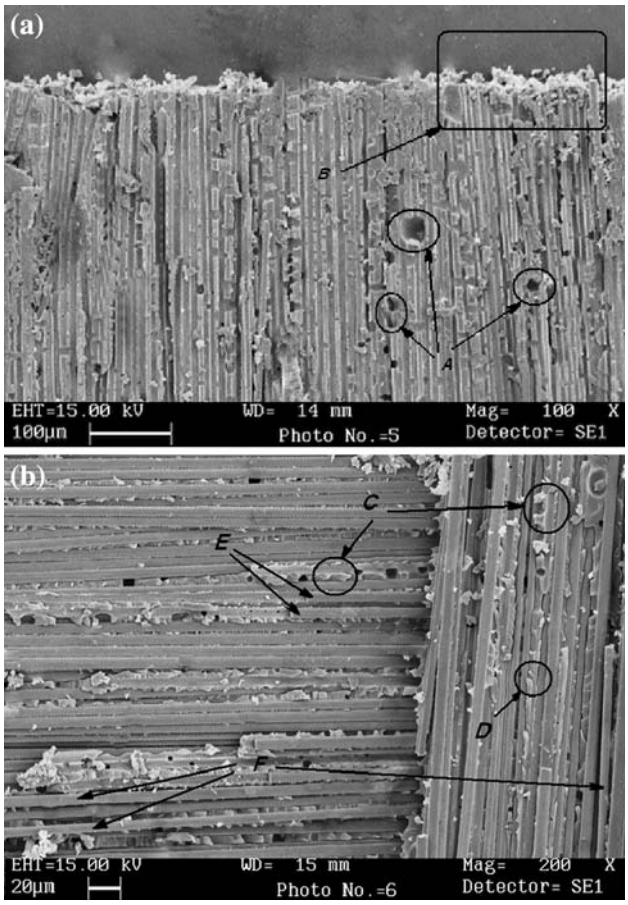

Fig. 13 **a** Initiation fracture surface, **b** propagation fracture surface of mixed mode loading of 45°

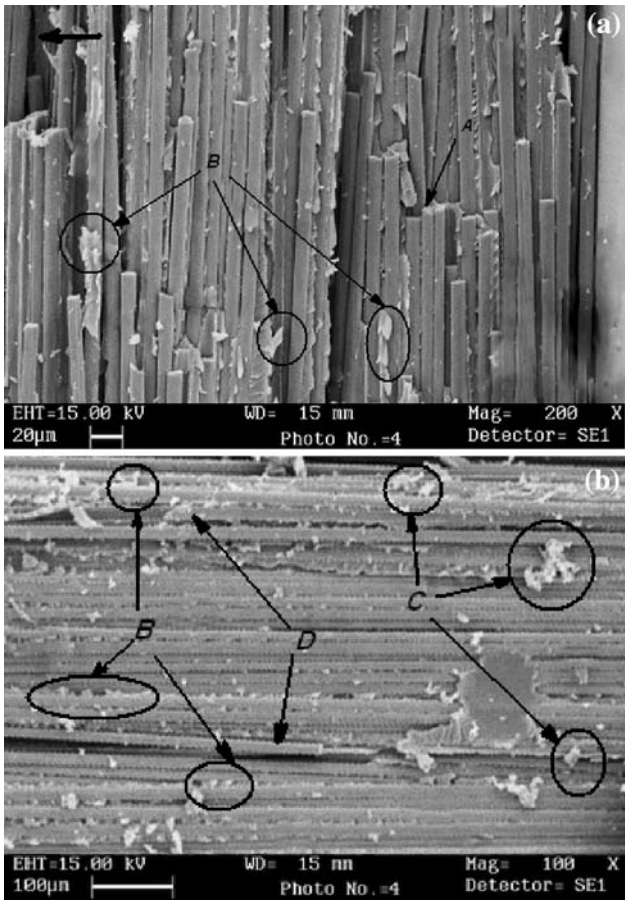

Fig. 14 **a** Initiation fracture surface, **b** propagation fracture surface of pure shearing mode

detected. The presence of voids with a smeared appearance indicates that ductile crack propagation conditions are favoured with respect to the mode-I specimen case because an increased shear deformation is allowed.

Conclusions

In this paper, the mixed-mode interlaminar fracture behaviour of carbon-epoxy composite specimens was investigated based on experimental and numerical analyses. A modified version of Arcan specimen was employed to conduct a mixed mode test using the special test loading device. The full range of mixed-mode loading conditions including pure mode-I and pure mode-II loading can be created and tested. It is a simple test procedure, clamping/unclamping the specimens is easy to achieve and only one type of specimen is required to generate all loading conditions.

The finite element results indicated that for loading angles close to pure mode-II loading, a high ratio of mode-II to mode-I fracture is dominant and there is an opposite trend for loading angles close to pure mode-I loading. It confirms that by varying the loading angle of Arcan specimen pure mode-I, pure mode-II and a wide range of mixed-mode loading conditions can be created and tested. Also, numerical results confirmed that the increase of the mode-II loading contribution leads to an increase of fracture resistance in the woven carbon-epoxy composite and the increase of the crack length leads to a reduction of interlaminar fracture resistance.

The interlaminar fracture toughness was determined experimentally with the modified version of the Arcan specimen under different mixed-mode loading conditions. Results indicated that the interlaminar cracked specimen is tougher in shear loading condition and weaker in tensile loading condition. A variety of models were investigated to choose an appropriate criterion to model woven carbon-epoxy composite responses. Exponential hackle criterion was the best criteria to use for this purpose. The arbitrary constant of γ, calculated through curve fitting and least square methods determined with the amount of $\gamma = 25.05$.

The fracture surfaces of the woven carbon-epoxy composite under different mixed-mode loading conditions were examined by scanning electron microscopy to gain insight into the failure responses. The SEM fracture surface observations showed that the mode-I fracture surface is indicative of a brittle cleavage failure with relatively smooth and flat matrix fracture and shows only a little debonding between fibre and matrix. As the mode-II loading contribution is added, the fracture surfaces become rougher and troughs and hackles appear. Everywhere on the mode-II fracture surface of the specimens, broken fibres, troughs and hackles were observed.

References

1. Dharmawan F, Simpson G, Herszberg I, John S (2006) Compos Struct 75:328
2. Reeder JR, Crews JR (1990) AIAA J 28:1270
3. Banks-Sills L, Freed Y, Eliasi R, Fourman V (2006) Int J Fract 141:195
4. Liu C, Huang Y, Lovato ML, Stout MG (1997) Int J Fract 87:241
5. Kim BW, Mayer AH (2003) Compos Sci Technol 63:695
6. Arcan M, Hashin Z, Voloshin A (1978) Exp Mech 18:141
7. Banks-Sills L, Arcan M, Bortman Y (1984) Eng Fract Mech 20(1):145
8. Jurf RA, Pipes RB (1982) J Compos Mater 16:386
9. Yoon SH, Hong CS (1990) Exp Mech 30:234
10. Choupani N (2008) Mater Sci Technol 478:229
11. Kinloch AJ, Wang Y, Williams JG, Yayla P (1993) Compos Sci Technol 47:225
12. Gilchrist MD, Svensson N, Shishoo R (1998) J Mater Sci 33:4049. doi:10.1023/A:1004431104540
13. Stevanovic D, Kalyanasundaram S, Lowe A, Jar PYB (2003) Compos Sci Technol 63:1949
14. Benzeggagh ML, Kenane M (1996) Compos Sci Technol 56(4):439
15. Ducept F, Davies P, Gamby D (1997) Compos A Appl Sci Manuf 28(8):719
16. Ducept F, Davies P, Gamby D (2000) Int J Adhes Adhes 20:233
17. Ducept F, Gamby D, Davies P (1999) Compos Sci Technol 59(4):609
18. Hashemi S, Kinloch AJ, Williams JG (1990) Compos Sci Technol 37:429
19. Kikuchi M, Kuroda M (1992) JSME Int J Ser 1 Solid Mech Strength Mater 35(4):496
20. Naik NK, Reddy KS, Meduri S, Raju NB, Prasad PD, Azad SNM, Ogde PA, Reddy BCK (2002) J Mater Sci 37(14):2983. doi:10.1023/A:1016025232102
21. O'Brien TK (1998) Compos B Eng 29(1):57
22. Rikards R, Buchholz F-G, Wang H, Bledzki AK, Korjakin A, Richard H-A (1998) Eng Fract Mech 61(3–4):325
23. Warrior NA, Pickett AK, Lourenc NSF (2003) Strain 39(4):153
24. American Society for Testing and Materials (1991) Standard D5045-91a, plane-stain fracture toughness and strain energy release rate of plastic materials, annual book of ASTM standards. ASTM, Philadelphia
25. ABAQUS (2004) ABAQUS user's manual, version 6.5. Hibbit, Karlsson and Sorensen, HKS Inc, Pawtucket, USA